The Astrophysical Journal, 952:141 (9pp), 2023 August 1 https://doi.org/10.3847/1538-4357/acdcf3

A Unique Low-mass-ratio Contact Eclipsing Binary System under the Period Cutoff

Athanasios Papageorgiou[1], Panagiota-Eleftheria Christopoulou[1], Eleni Lalounta[1], C. E. Ferreira Lopes[2,3], Márcio Catelan[4,5,6], Andrew J. Drake[7], Panayiotis Hantzios[8], and Ioannis Alikakos[8]
[1] Department of Physics, University of Patras, 26500, Patra, Greece; apapageorgiou@upatras.gr
[2] Instituto de Astronomía y Ciencias Planetarias, Universidad de Atacama, Copayapu 485, 1531772 Copiapó, Chile
[3] Instituto Nacional de Pesquisas Espaciais (INPE/MCTI), Av. dos Astronautas, 1758, São José dos Campos, SP, 12227-010, Brazil
[4] Instituto de Astrofísica, Facultad de Física, Pontificia Universidad Católica de Chile, Av. Vicuña Mackenna 4860, 7820436 Macul, Santiago, Chile
[5] Millennium Institute of Astrophysics, Nuncio Monseñor Sotero Sanz 100, of. 104, 7500000 Providencia, Santiago, Chile
[6] Centro de Astroingeniería, Facultad de Física, Pontificia Universidad Católica de Chile, Av. Vicuña Mackenna 4860, 7820436 Macul, Santiago, Chile
[7] California Institute of Technology, 1200 East California Boulevard, Pasadena, CA 91225, USA
[8] Institute for Astronomy, Astrophysics, Space Applications and Remote Sensing, National Observatory of Athens, 15236, Athens, Greece
Received 2023 April 24; revised 2023 June 7; accepted 2023 June 7; published 2023 July 25

Abstract

We present a multiband photometric analysis of CRTS J163819.6+03485, the first low-mass-ratio contact binary system with a period of 0.2053321 day under the contact binary period limit. The unprecedented combination of mass ratio and period makes this system unique for eclipsing binary (EB) research. Using new multiband photometric observations, we explored the parameter space of this unique total EB system through a detailed scan in the mass ratio–inclination plane and using the PIKAIA genetic algorithm optimizer. The best set of relative physical parameters and corresponding uncertainties was adopted through Markov Chain Monte Carlo sampling of the parameter space. The resulting mass ratio of the system is $q = 0.16 \pm 0.01$. The absolute parameters were derived by adopting an empirical mass–luminosity relation. Period changes are also investigated by using new observations and archival photometric light curves from massive astronomical surveys, which revealed in a preliminary solution the presence of a possible low-mass tertiary companion. The origin and evolutionary status of the system are investigated through the detached binary formation scenario.

Unified Astronomy Thesaurus concepts: Eclipsing binary stars (444); Astronomy data analysis (1858); W Ursae Majoris variable stars (1783); Astronomy data modeling (1859); Fundamental parameters of stars (555)

1. Introduction

In the era of large sky surveys, where a plethora of new contact binaries are discovered and analyzed through automated processes, ultrashort-period and low-mass-ratio systems remain two of the most enigmatic classes that challenge current theoretical models. Ultrashort-period contact binaries (USPCBs) remain important, as they allow investigation of the evolution of low-mass contact binary stars under the well-known orbital period cutoff, located at approximately 0.22 days (Rucinski 1992) or slightly lower (∼0.15–0.20 day; Li et al. 2019). Low-mass-ratio contact binaries (LMRs; $q \leqslant 0.25$) are of particular interest, as the process of exchanging mass and angular momentum (AM) between the components can dramatically alter the evolution of both stars, giving rise to tidal instabilities and finally leading them to coalesce. Our review of LMRs (Christopoulou et al. 2022) with a spectroscopic determination of mass ratios or/and total eclipses revealed that the majority have periods around 0.4 day. With the same criteria, our compilation of USPCBs revealed a concentration of mass ratio of around 0.4 (Papageorgiou et al. 2023).

CRTS_J163819.6+034852, with coordinates R.A.(J2000) = $16^h38^m19.67^s$, decl.(J2000) = +03°48′51.64″ and a period of 0.205332 day, is one of the shortest-period contact binaries found in the Catalina Sky Survey (CSS; Drake et al. 2014). From an analysis of All-Sky Automated Survey for Supernovae (ASAS-SN) observations (Shappee et al. 2014), Jayasinghe et al. (2018) reported a period of 0.2053318 day, a *V*-band mean magnitude of 14.51 mag, and an amplitude of 0.39 mag. Christopoulou et al. (2022) found that it is also an extreme LMR system, making this system one of a kind, since it is, to our knowledge, the only one with this rare combination of period and mass ratio.

Here we present the first multiband follow-up photometric observations of this unique binary (hereafter, CRTS_J163819) in combination with archival light curves (LCs) from other surveys, carrying out a period analysis spanning 15 yr, with the intent to clarify its nature.

2. Observations

2.1. New Photometric Observations

We observed CRTS_J163819 in two observing runs in 2018 and 2021 with the 2.3 m Ritchey-Chrétien Aristarchos telescope at Helmos Observatory, Greece. In the first run, on 2018 July 3, as our primary goal was to confirm its short period, we observed CRTS_J163819 using a broad VR filter with the RISE-2 CCD camera. RISE-2 has a CCD size of 1k × 1k, with a pixel scale of 0.″6 and a field of view of 10′ × 10′. For the second run, on 2021 June 25, 26, and July 2 and 3, we observed in *B*, *V*, *R*, *I* for 180 s, 90 s, 40–50 s, and 60–70 s, respectively, with a liquid-nitrogen-cooled Princeton Instruments VersArray CCD camera. This CCD camera has 1024 × 1024 pixels, with an effective field of view of 4.′8 × 4.′8.

For the preprocessing of raw images (bias subtraction and flat-fielding) and the aperture photometry, we used our fully

automated pipeline (Papageorgiou & Christopoulou 2015) that incorporates PyRAF (Science Software Branch at STScI 2012) and the Astrometry.net packages (Lang et al. 2010). The differential LCs were generated after choosing suitable comparison and check stars close to the target star in the field. These are 2MASS J16382385+0350508 ($J = 13.532 \pm 0.029$ mag, $H = 13.175 \pm 0.022$ mag, $K = 13.110 \pm 0.035$ mag) and 2MASS J1638176+0349143 ($J = 12.302 \pm 0.024$ mag, $H = 12.033 \pm 0.027$ mag, $K = 11.999 \pm 0.026$ mag), respectively. The typical errors in the final differential magnitudes throughout the observing run are 8−10 mmag.

2.2. Photometric Observations from Astronomical Sky Surveys

LCs of CRTS_J163819 were also found in ASAS-SN (in the *V* filter; Shappee et al. 2014; Jayasinghe et al. 2018), CSS (Drake et al. 2014), Zwicky Transient Facility (ZTF,[9] in *g* and *r*; Masci et al. 2019), and the Asteroid Terrestrial-impact Last Alert System (ATLAS,[10] *o* and *c* bands; Heinze et al. 2018) variable star catalog.

3. LC Modeling

Our new *BVRI* LCs of CRTS_J163819 (Figure 1(c)) show a typical W UMa-type eclipsing binary (EB) system with total eclipses. Given that radial velocity curves are not available, we employed the PHOEBE-0.31a scripter (Prša & Zwitter 2005) to analyze our four-color LCs simultaneously and derive a reliable photometric mass ratio, $q = \frac{M_2}{M_1}$, taking advantage of the totality (Terrell & Wilson 2005; Hambálek & Pribulla 2013; Şenavcı et al. 2016). Assuming circular orbits under "Overcontact not in thermal contact" mode, we performed a detailed scan in the mass ratio–inclination ($q - i$) plane using a grid of predefined values. The mass ratio was selected in the range of [0.1–3.0], with a 0.01 resolution, with the inclination in the range of [68°–90°], using 1° steps. The LCs were weighted according to their errors. The effective temperature of the primary (star eclipsed at phase zero) was set equal to the system's temperature, $T_{\rm eff} = 6662 \pm 162$ K, as given by the Transiting Exoplanet Survey Satellite Input Catalog Version 8 (Stassun et al. 2019). The adopted gravity-darkening coefficients and bolometric albedos were $A_{1,2} = 0.5$ (Ruciński 1973) and $g_{1,2} = 0.32$ (Lucy 1967), respectively, and the bolometric and bandpass limb-darkening coefficients were interpolated from van Hamme (1993) tables with a logarithmic law. In order to reach convergence, the Method of Multiple Subsets (Wilson & Biermann 1976) was used, adjusting the passband luminosity L_1 and the temperature of the secondary component (T_2) or the modified surface equipotentials ($\Omega_{12} = \Omega_1 = \Omega_2$) for 20 iterations each set. Finally, parameters Ω_{12}, T_2, and L_1 were adjusted together to converge for 50 iterations.

We follow the fitting strategy of Christopoulou et al. (2022). The corresponding photometric parameters from our LC modeling, along with their errors calculated via a Monte Carlo (MC) procedure, are listed in column 2 of Table 1. The mass ratio ($\log q$) versus cost function value ($\log \chi^2$) derived from the $q - i$ scan method is shown in Figure 1(a).

To explore further the parameter space and the uncertainties of the model parameters, we used a genetic algorithm (GA) optimizer technique. Specifically, we apply the PIKAIA GA (Charbonneau 1995) interfaced with PHOEBE, as adapted in Papageorgiou (2015) and Papageorgiou et al. (2023). The population size was set to 120 individuals, and 2000 generations were computed. The best-fit parameters as defined by the best individuals from this list are $q = 0.16 \pm 0.012$, $i = 85\overset{\circ}{.}3 \pm 3\overset{\circ}{.}5$, $T_2/T_1 = 0.972 \pm 0.026$, $\Omega_{12} = 2.062 \pm 0.028$, $r_1 = 0.570 \pm 0.009$, and $r_2 = 0.271 \pm 0.017$. Furthermore, to determine the uncertainties more robustly, we used the affine-invariant Markov Chain Monte Carlo (MCMC) ensemble sampler implemented in the EMCEE (Foreman-Mackey et al. 2013) Python package, coupled with the 2015 version of the Wilson–Devinney (W-D) binary star modeling code (Wilson & Devinney 1971; Wilson et al. 2020).[11] The values of q, i, T_r, $\Omega_{1,2}$, and L_1, as determined by the $q - i$ scan and GA optimizer, were served as priors for the MCMC sampling. A total of 30 walkers were used. The MCMC parameter search was run for 6000–10,000 steps, with a burn-in phase of 1500–2000 steps, for our *BVRI* LCs, resulting in ∼180,000 iterations. Figures 1(b) and (c) show the probability distributions of q, i, T_r, $\Omega_{1,2}$, and the theoretical synthetic models (solid lines), respectively. The final parameters with their uncertainties, listed in the third column of Table 1, are obtained using the mean value and the standard deviation.

4. Period Variation Analysis

Due to the absence of available times of minimum light (ToMs) of CRTS_J163819, we exploited the information provided from large astronomical surveys (CSS, ASAS-SN, ZTF, and ATLAS) by collecting the publicly available LCs. This information not only provides insight into the LC evolution history, but also valuable information on the period variation over a time span of more than 15 yr (2004–2021). Figure 1(d) shows the archival LCs of in different passbands, mined from CSS, ASAS-SN, ZTF, and ATLAS, and the LC from the broad RISE-2 VR filter observed on 2018 July 3. The model derived in Section 3 is overplotted on CSS and ASAS-SN in *V* band. The models for the ZTF *g* and *r* bands were constructed using PHOEBE-2 (Prša et al. 2016) with our solution parameters. The RISE-2 and ATLAS LCs were used only to derive 88 ToMs, since they are obtained in VR, "cyan" (c) and "orange" (o) wide filters, respectively.

Instead of using phenomenological models for ToM calculations that have been proven efficient when dealing with a large number of LCs (Li et al. 2018; Hajdu et al. 2019; Papageorgiou et al. 2021), we take advantage of the constructed models for each archival and new photometric data set, and we calculate the ToM by applying the semi-automatic fitting procedure (Zasche et al. 2014). All 275 ToMs are converted to Heliocentric Julian Dates (HJD). In the case of surveys with low time resolutions (low cadences), we used longer-time-span data to construct the full-phase LC. Therefore, a linear ephemeris for CRTS_J163819 was derived using the new ToM, as follows:

$$\mathrm{MinI} = 2459692.76790 + 0.2053321 \times E, \quad (1)$$

where MinI is the HJD ToM at epoch E. To study the orbital period variation for the first time, we calculate all available ToMs with Equation (1) and estimate the observed minus computed ($O - C$) ToMs (Figure 2). As can be seen in this figure, the $O - C$ curve shows a combination of a downward

[9] https://irsa.ipac.caltech.edu/
[10] https://atlas.fallingstar.com/
[11] ftp://ftp.astro.ufl.edu/pub/wilson/lcdc2015/

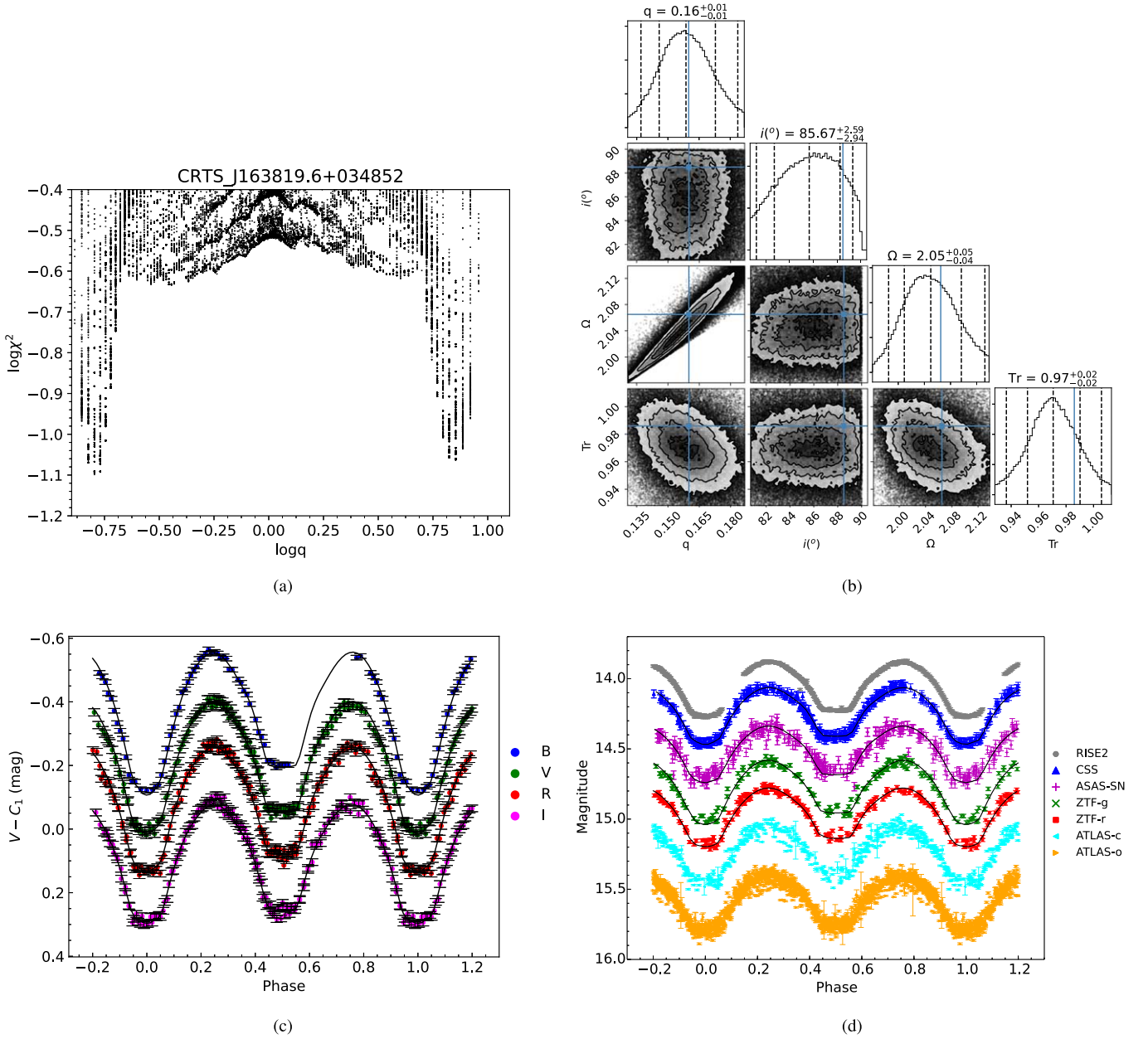

Figure 1. (a) Mass ratio ($\log q$) vs. cost function value ($\log \chi^2$) derived from the $q - i$ scan method, as applied to CRTS_J163819. (b) The probability distributions (Foreman-Mackey et al. 2013) of q, i, Ω, and T_r, determined by the MCMC modeling. The blue lines represent the solution of the system from the $q - i$ method. (c) The new observed folded LCs from the Aristarchos telescope and synthetic models of CRTS_J163819 (solid lines). The B, I LCs are shifted vertically for clarity, by $B + 0.2$ and $I + 0.1$, respectively. (d) Photometric data (with errors) of CRTS_J163819.6, folded with respect to the period of 0.205332 day.

parabola and a nearly sinusoidal variation. Therefore, we incorporate in the eclipse time variation (ETV) model both a parabolic and a light travel time effect (LTTE) term, following Irwin (1952), due to mass transfer and a possible tertiary companion, respectively:

$$O - C = \Delta T_o + \Delta P_o \times E + Q \times E^2 + \tau_3, \quad (2)$$

where ΔP_o and ΔT_o are the corrections of the initial period and primary minimum with respect to the values in Equation (1), Q is the long-term rate of change in orbital period, and τ_3 is the LTTE due to a circumbinary companion (Irwin 1952). The latter includes the projected semimajor axis $\alpha_b \sin i_3$ (or semi-amplitude of the LTTE, A), eccentricity e_b, the argument of the periastron of the orbit ω_b, the true anomaly υ_b of the position of mass center, and the time of periastron passage T_p, all of which refer to the EB's center of mass around the center of mass of the triple system. The period P_3 and the time of periastron passage T_p are included when solving Kepler's equations.

To solve for the eight parameters (ΔT_o, ΔP_o, Q, A, e_b, ω_b, P_3, and T_p), we initialize the model parameters by fitting the ETV model coupled with the PIKAIA GA. We evolved a population of 120 sets of parameters randomly generated from uniform distributions, for 1000 generations. The mean parameter values from the last generation were used as input parameters, and a least squares (LS) fitting was performed. The model rapidly converged to a solution within 1σ of the GA initial solution. We estimate the model parameter errors by performing a final fitting via an MCMC procedure. This was done by using the PYMC (Fonnesbeck et al. 2015) package in

Table 1
The System Parameters and Uncertainties for CRTS_J163819.6+034852

	Physical Parameters		Approximate Absolute Parameters	
	$q-i$ Scan	MCMC		
$q=\frac{M_2}{M_1}$	0.16 ± 0.02	$0.16^{+0.01}_{-0.01}$	$T_{\rm sys}(K)$	6662 ± 200
$T_r=\frac{T_2}{T_1}$	0.986 ± 0.006	$0.971^{+0.020}_{-0.019}$	$\alpha(R_\odot)$	1.63 ± 0.01
$R_r=\frac{R_2}{R_1}$	0.466 ± 0.006	$0.472^{+0.012}_{-0.012}$	$T_1(K)$	6696 ± 202
r_1	0.567 ± 0.009	$0.572^{+0.011}_{-0.012}$	$T_2(K)$	6502 ± 234
r_2	0.264 ± 0.008	$0.270^{+0.005}_{-0.006}$	$M_1(M_\odot)$	1.19 ± 0.02
Ω_{12}	2.065 ± 0.008	$2.050^{+0.047}_{-0.041}$	$M_2(M_\odot)$	0.19 ± 0.02
$i(^\circ)$	88.5 ± 1.2	$85.7^{+2.6}_{-2.9}$	$R_1(R_\odot)$	0.93 ± 0.02
$f(\%)$	63 ± 8	72^{+14}_{-17}	$R_2(R_\odot)$	0.44 ± 0.01
$\frac{L_{1B}}{L_{B\rm tot}}$	0.837 ± 0.002	$0.846^{+0.013}_{-0.013}$	$L_1(L_\odot)$	1.45 ± 0.07
$\frac{L_{1V}}{L_{V\rm tot}}$	0.835 ± 0.002	$0.841^{+0.010}_{-0.011}$	$L_2(L_\odot)$	0.31 ± 0.05
$\frac{L_{1R}}{L_{R\rm tot}}$	0.833 ± 0.002	$0.839^{+0.009}_{-0.009}$	$M_{\rm bol,1}$(mag)	4.34 ± 0.05
$\frac{L_{1I}}{L_{I\rm tot}}$	0.831 ± 0.002	$0.837^{+0.008}_{-0.008}$	$M_{\rm bol,2}$(mag)	6.01 ± 0.18
	ETV Model			
P_3(yr)	29^{+12}_{-9}		T_p(days)	2457542 ± 123
A (days)	0.0058 ± 0.0014		Q (days cycle^{-1})	$(-4.0\pm0.1)\times10^{-11}$
$a_b\sin i_3$(AU)	1.2 ± 0.3		$f(M_3)(M_\odot)$	0.00022
e_3	0.68 ± 0.10		$M_3(M_\odot)$ (90°)	0.18
$\omega_b(^\circ)$	328 ± 10		$a_3(AU)(90^\circ)$	9.4 ± 2.3

Note. q, T_r, and R_r are the mass, temperature, and radius ratios of the two components, respectively; $\frac{L_{1j}}{L_{j\rm tot}}$ is the fractional luminosity of the primary component in filter j; i is the orbital inclination; Ω_{12} is the potential of the components; r_1 and r_2 are the mean relative radii; and $f=\frac{\Omega-\Omega_{\rm in}}{\Omega_{\rm out}-\Omega_{\rm in}}$ is the fillout factor, where $\Omega_{\rm in}$ and $\Omega_{\rm out}$ are the modified Kopal potential of the inner and the outer Lagrangian points, respectively. A is the semi-amplitude of LTTE; $\omega_3=\omega_b-\pi$ is the argument of the periastron of the third body; and a_3 denotes the semimajor axis of the potential third body around the center of mass of the triple system, for $i_3=90^\circ$. The rest of the parameters of the ETV model are described in the text.

Python. The model parameters were sampled from uniform distributions centered at the LS solution, with 2σ ranges as provided by the GA solution. To avoid biases in the initial solution, a burn-in period was set to 20,000 iterations (200,000 iterations in total). Figure 2 shows the final model, overplotted on the $O-C$ diagram. The derived parameters are listed in Table 1.

5. Results

The photometric parameters determined from different methods ($q-i$ search, heuristic scan with parameter perturbation/MC with PHOEBE, MCMC sampler with W-D, and PIKAIA GAs with PHOEBE) are consistent, within the reported errors. To determine the masses (M_1, M_2), radii (R_1, R_2), and luminosities (L_1, L_2) of the components, we use the results and the uncertainties of the MCMC sampler, following the method proposed in Christopoulou et al. (2022), using the distance given by Gaia Data Release 3 (DR3; Gaia Collaboration 2022) as 939 ± 15 pc. The primary's mass was estimated by the mass–luminosity approximation (for details, see Christopoulou et al. 2022; Papageorgiou et al. 2023):

$$\log L_1=\log(0.63\pm0.04)+(4.8\pm0.2)\log M_1. \quad (3)$$

The approximate absolute parameters of the binary components are listed in the fifth column of Table 1.

If the periodic component of CRTS_J163819 eclipse timings is interpreted as the LTTE due to a circumbinary companion, the minimum mass ($i_3=90^\circ$) is found to be $M_3=0.18\,M_\odot$ at a separation from the binary $\sim$11.0 au ($\alpha_b+\alpha_3$ for $i_3=90^\circ$; Table 1). If it is a main-sequence star, it would have a temperature of 3100 K and a bolometric luminosity $0.003\,L_\odot$. Thus, the contribution to the total light of the system would be $L_3/(L_1+L_2+L_3)=0.002$. Accordingly, in agreement with our results, the tertiary companion may not be detected as a third light source in the LC analysis. We computed also the semi-amplitude of the third-body dynamic perturbation on the binary orbit, finding it to be negligible. The quadratic term in the analysis of the $O-C$ diagram represents a continuous decrease at a rate of -7.11×10^{-8} days yr^{-1}. Such a variation could be the result of mass transfer from the more massive component (primary) to its secondary companion or angular momentum loss (AML) due to a magnetic stellar wind. Considering conservative mass transfer, the transfer rate is $dM_1/dt=-2.61\times10^{-8}M_\odot$ yr^{-1}, typical for mass-transferring USPCBs (Li et al. 2020) and LMRs (Li et al. 2021). Assuming that the transfer is produced on a thermal timescale, $\tau_{\rm th}=3.24\times10^7$ yr, the mass is transferred to the companion at a rate of $M_1/\tau_{\rm th}=3.67\times10^{-8}M_\odot$ yr^{-1}. This value is similar to that calculated from the period analysis, making mass transfer a possible cause. We also examined AML via a magnetized wind as a possible mechanism for the period decrease, using equation (23) of Stepien (1995). We found the AML rate to be two orders of magnitude smaller than the observed dP/dt value. This suggests that magnetic braking is not the main cause of period decrease.

An alternative explanation of the orbital period modulation of the CRTS_J163819 system is strong magnetic activity due to the Applegate effect (Applegate 1992). Using the Völschow

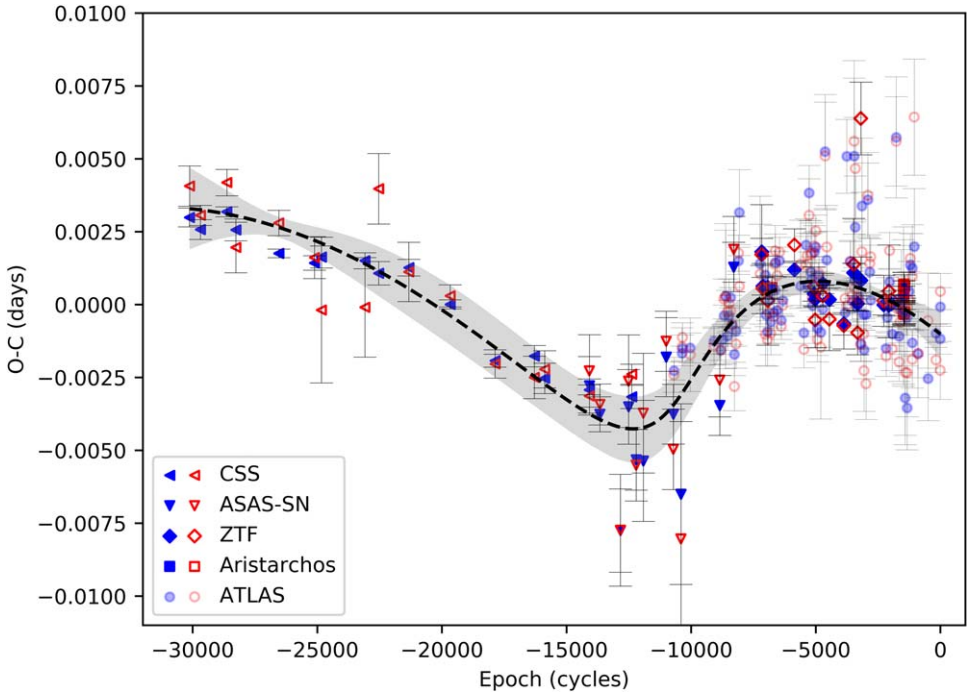

Figure 2. $O-C$ diagram of CRTS_J163819, computed with respect to the linear terms of Equation (1). The dashed line represents the full contribution of the quadratic-plus-LTTE ephemeris, with the shading being indicative of the 1σ uncertainty. The blue filled and red hollow symbols represent the primary and secondary ToMs, respectively.

et al. (2016) eclipsing time variation calculator[12] and the absolute physical parameters of the components given in Table 1, we found that the energy ΔE required to drive the Applegate mechanism is 29% of the available energy $E_{\rm sec}$, produced in the magnetically active secondary star for the finite-shell two-zone model (Völschow et al. 2016) or 1.5% for the thin-shell model (Tian et al. 2009). Therefore, for CRTS_J163819, since $\Delta E/E_{\rm sec} < 1$, the Applegate mechanism appears to be energetically feasible. However, for a rapidly rotating secondary with a convective envelope, we expect signs of dynamo activity, such as starspots (or other chromospheric manifestations), which typically manifest themselves in the LCs by an asymmetry between maxima (the O'Connell effect). We did not detect the presence of unequal maxima in the LCs or any source of UV or X-ray emission within $2''$ of the position of CRTS_J163819 in the relevant catalogs.

However, we have to note that since the time span of the available data from the astronomical surveys covers the half cycle of the total outer orbit, we consider this model as highly preliminary to the outer orbit determination.

6. Discussion and Conclusions

The first photometric solution revealed that CRTS_J163819 has an extremely low mass ratio, $q = 0.16 \pm 0.01$, which makes this system unique among LMRs and USPCBs, given that its period (0.205332 day) is also under the contact period limit of 0.22 day (Figure 3(a)). The fillout factor ($72\% \pm 15\%$) suggests that the system is in deep contact, and the temperature difference between the components indicates that they are under thermal contact. It appears to be an A-subtype EB, in which a primary of $F5/F4$ spectral type is eclipsed during the deeper minimum. We note, however, that spectroscopic studies of this system will ultimately be needed to more robustly determine the mass ratio. In this regard, we note that there is generally very good agreement between photometric and spectroscopic mass ratios in totally eclipsing contact EBs (Li et al. 2021). Though we should point out that according to Rucinski (2020), the discrepancy between the spectroscopic and photometric mass ratio can be as large as 10% and in some cases even larger (AW UMa). In other cases, e.g., ϵ CrA, although the photometric mass ratio $q_{\rm ph} = 0.128 \pm 0.0014$ is within 4σ of the spectroscopic value $q_{\rm sp} = 0.13 \pm 0.001$ and the discrepancy is minor, the detection of similar complex velocity flows as in AW UMa may imply the necessity of modifying the Roche lobe-based photometric mode (Rucinski 2020).

Figure 3(b) shows the positions of the two components of CRTS_J163819 on the $\log M - \log R$ diagram, along with other USPCBs compiled by Papageorgiou et al. (2023). The zero-age main sequence (ZAMS) and the terminal-age main sequence (TAMS), calculated for different metallicities using the Binary Star Evolution (BSE) code (Hurley et al. 2002), are overplotted. According to the locations of USPCB primaries with respect to ZAMS, the more massive primary star of CRTS_J163819 seems to act as a normal main-sequence star with relatively low metallicity. The secondary, less massive component is located beyond the TAMS, in accordance with the positions of other USPCB secondaries.

We also evaluated the potential progenitor of CRTS_J163819 as an ordinary detached system, using the evolutionary model of Stepien (2006; details of the model's construction are provided in Appendix).

Although the structure and detailed evolutionary process during the contact phase are still open questions, we can only point out that CRTS_J163819, having very low q and P, must be at a late stage of evolution. As it has a high fillout factor ($\geqslant 72\%$), we can consider it as the progenitor of a merger that

[12] http://theory-star formation-group.cl/applegate/index.php

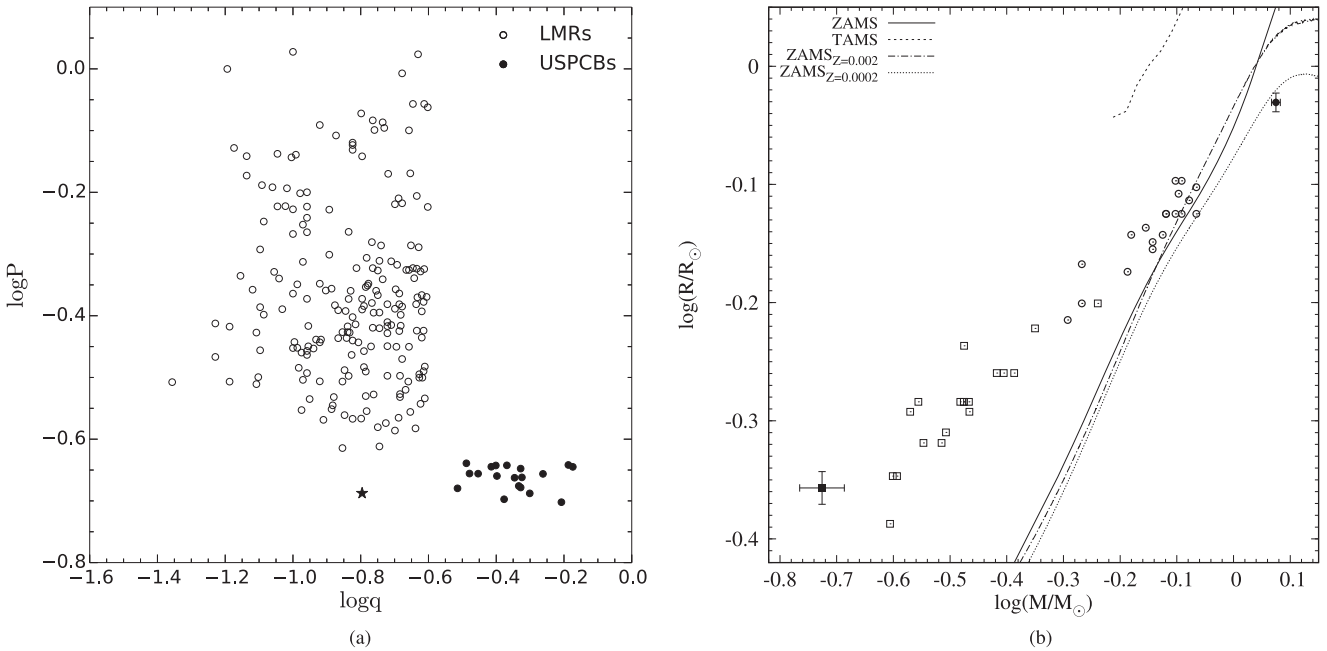

Figure 3. (a) Distribution of LMRs (open circles; from Christopoulou et al. 2022) and USPCBs (filled circles; from Papageorgiou et al. 2023) in the $\log q - \log P$ plane. The star symbol represents CRTS_J163819. (b) The primary and secondary components (filled circles and squares, respectively) of CRTS_J163819 compared with primary and secondary components (open circles and squares, respectively) of USPCBs (Papageorgiou et al. 2023), plotted on the $\log M - \log R$ diagram. ZAMS loci for different metallicities (the solid, dashed–dotted, and dotted lines), along with a TAMS locus (the dashed line) for solar metallicity, as obtained using the BSE code (Hurley et al. 2002), are overplotted.

will ultimately lead to an FK Com-like fast-rotating single star, blue straggler, or red nova (see, e.g., Rasio 1995; Tylenda et al. 2011; Stępień & Kiraga 2015). To investigate its stability, we calculate the ratio of the spin AM (J_s) to the orbital AM (J_o; assuming corotation of the component's spin and the orbit) to be $J_s/J_o = 0.145$, using values of $k_1^2 = k_2^2 = k^2 = 0.06$ (Rasio 1995) for the gyration radii of both components. Alternatively, $J_s/J_o = 0.154$ using $k_2^2 \sim 0.205$ and evaluating $k_1^2 = 0.058$ from Christopoulou et al. (2022) for a star of $1.19\,M_\odot$. In both cases, J_s/J_o does not exceed the instability value of ∼one-third (Darwin's instability; see, e.g., Hut (1980), and references therein), indicating that the system is in a stable state at present. Nevertheless, CRTS_J163819 has the highest value of J_s/J_o among USPCBs (see Appendix). To further investigate its stability, we calculate the theoretical instability mass ratio ($q_{inst} = 0.088$), the instability separation ($a_{inst} = 1.269\,R_\odot$), and the instability period ($P_{inst} = 0.141$ day), by applying the method of Wadhwa et al. (2021), using $k_2^2 \sim 0.205$ and $k_1^2 = 0.058$, as above. All three resulting parameters are smaller than the corresponding current parameters, suggesting that CRTS_J163819 is a stable binary for now.

According to this approach, there is no single value to the limit of the mass instability ratio, as it depends on the primary mass for low-mass stars, and therefore on the different structures of tidally deformed and rotating ZAMS stars, metallicity, and age. However, the inability to explain why systems such as V1187 Her and V857 Her violate the theoretical limits highlights the need to extract more reliable mass ratios from radial velocity curves and/or the need to understand and model the stationary flow structures (Rucinski 2020). Why is CRTS_J163819 the only such system to be observed so far? Why are systems with this combination of q and P so rare? To investigate these issues, we need future spectroscopic observations of the radial velocities of the components to establish the mass ratio. Furthermore, the measurement of the radial velocity would be useful to compute the space motions of CRTS_J163819 to infer its kinematical age through age–velocity dispersion relations.

Acknowledgments

Based on observations made with the 2.3 m Aristarchos telescope, Helmos Observatory, Greece, which is operated by the Institute for Astronomy, Astrophysics, Space Applications and Remote Sensing of the National Observatory of Athens, Greece. This research is cofinanced by Greece and the European Union (European Social Fund, ESF) through the Operational Programme "Human Resources Development, Education and Lifelong Learning" in the context of the project "Reinforcement of Postdoctoral Researchers—2nd Cycle" (MIS-5033021), implemented by the State Scholarships Foundation (IKY). E.L. gratefully acknowledges the support provided by IKY "Scholarship Programme for PhD candidates in the Greek Universities." M.C. and C.E.F.L. acknowledge the support provided by ANID's Millennium Science Initiative through grant ICN12_12009, awarded to the Millennium Institute of Astrophysics (MAS). Additional support for M.C. is provided by ANID Basal project FB210003. This research has made use of the VizieR catalog access tool, CDS, Strasbourg, France. We would like to thank Prof. K. Stepien for his useful comments/suggestions for the models of progenitors. We would like to thank the referee for constructive comments and recommendations that have improved the paper.

Facilities: Aristarchos 2.3 m, ZTF, ASSAS-SN, CSS.

Software: PHOEBE-0.31A (Prša & Zwitter 2005), PHOEBE-2 (Prša et al. 2016), EMCEE (Foreman-Mackey et al. 2013), W-D CODE (Wilson et al. 2020), TRIANGLE.PY-V0.1.1 (Foreman-Mackey et al. 2014), PYMC (Fonnesbeck et al. 2015),

MWDUST (Bovy et al. 2016), PYRAF (Science Software Branch at STScI 2012), ASTROMETRY.NET (Lang et al. 2010).

Appendix
Models of Progenitors of CRTS_J163819

Although there have been a few studies on the structure or evolution of contact binaries via the detached channel (Yakut & Eggleton 2005; Jiang et al. 2014; Jiang 2020), taking into account the complex physical processes (spin, orbital rotation, tides, mass and energy exchange, and AML due to magnetic braking), for most of the models the examples were stopped as soon as contact was reached. To approximate the progenitors of the current system, we adopted the scenario proposed by Stepien (2006) and (Stępień & Kiraga 2015, and references therein), which can predict the observational phenomena and the parameters of cool low-mass contact binaries. This scenario describes the evolution of a detached binary of two magnetically active MS stars with circular, coplanar, and synchronized orbits from ZAMS to a phase just before the components merge or form a common envelope. Neglecting any interaction between the winds or other mechanisms (a possible tertiary companion), the dominating mechanisms of the orbit evolution are the magnetic braking due to the winds and the mass transfer between the components. Three phases make up the evolutionary calculations: the first phase considers a detached binary, during which the more massive component (donor) evolves from ZAMS to the Roche lobe overflow (RLOF); the second phase considers a rapid, conservative mass exchange from the donor to a less massive component (the accretor); and the third phase considers a slow mass transfer to the accretor as a result of the nuclear evolution of the donor. The mathematical description of the model is given more fully in Section 2.1 of Stępień & Kiraga 2015; see Equations (1)–(8)). The set of eight basic equations of the model are the third Kepler law, the standard expression for binary rotational and orbital AM, the following formulas that predict how much mass and AM the winds carry away, and the approximate expressions for inner Roche lobe sizes (Eggleton 1983):

$$\frac{dM_{1,2}}{dt}\,[M_\odot\ \mathrm{yr}^{-1}] = 10^{-11}R_{1,2}^2, \tag{A1}$$

$$\frac{dJ_{\mathrm{tot}}}{dt}\,[\mathrm{g\ cm^2 s^{-1} yr^{-1}}] = -4.9\times 10^{41}(\mathrm{R_1^2 M_1 + R_2^2 M_2})/\mathrm{P}, \tag{A2}$$

where $M_{1,2}$, $R_{1,2}$ are the masses and radii of both components and J_{tot} is the total (orbital and rotational) AM. This scenario entails the following basic assumptions:

1. Because we lack detailed evolutionary models of binary components during and after the mass exchange, regardless of the details of the mass transfer process, both stars are assumed to retain thermal equilibrium at every step and phase. The set of eight equations is integrated at every time step and all stellar parameters are interpolated from the PAdova and TRieste Stellar Evolution Code (PARSEC; Bressan et al. 2012) grid, thus from a single-star evolutionary model.
2. Equations (A1) and (A2) are calibrated using observational information about the rotation of single, magnetically active stars of various ages and empirically calculated mass-loss rates of single, solar-type stars (Stepien 2006). The constant in Equation (A1) is uncertain within a factor of 2 and that in Equation (A2) is uncertain to ±30%. The binary system can reach contact while both components are still on the MS (the massive component reaches RLOF just reaching TAMS) after a rapid mass exchange, until the mass ratio reversal.
3. The evolution path to contact is determined by: (a) the initial values of the masses of the progenitor cool detached binary and its initial period; (b) the adopted mass transfer rate at the first overflow (when the initial massive component of the detached phase fills the Roche lobe for the first time, RLOF) and after mass ratio reversal; and (c) the metallicity, as it determines the MS lifetime and thus the time needed for the massive component to reach RLOF.
4. The first (rapid) constant mass transfer rate during Phase II (after RLOF of the initially more massive component) is adopted based on the observation that the total mass transferred in any of the modeled binary did not exceed half solar mass, assuming that the mass is transferred at a thermal timescale of 10^8 yr. As Stepien (2006) suggests, after trying many formulas of mass transfer, the best-adopted values that secured stability for most of the models were around $5\times 10^{-9}\,M_\odot\,\mathrm{yr}^{-1}$.
5. In Phase III (the beginning of the contact configuration), the influence of AML balances the mass transfer rate, so that the orbit remains tight. Thus, the mass transfer rate resulted from the comparison of the radius of the accretor (the secondary component) to the Roche lobe, in order to keep its contact configuration, and the radius of the primary was assumed to increase a little due to evolutionary effects. The correct value of the mass transfer rate required very fine tuning, not only to maintain the contact configuration, but also to shorten the orbital period. The mass is transferred at a rate proportional to the excess of the donor's size above the Roche lobe. The resulting values lie in the interval $3\text{–}4\times 10^{-10}\,M_\odot\,\mathrm{yr}^{-1}$, i.e., they are about 10 times lower than in Phase II.

Although, without an accurate binary age, its progenitor cannot be uniquely determined, the current observed total mass of CRTS_J163819 restricts the initial total progenitor mass to the range of 1.35–1.4 $M_\odot$, because the expected mass loss due to wind is typically less than 0.1 $M_\odot$ (Stępień & Kiraga 2015). In Figure 4(a), we present period tracks of old sets of models (1a–c and 2a–b) in the $P-q$ plane, together with other known USPCBs from Papageorgiou et al. (2023) and new models 3a–c. The latter describes the evolution of a close binary with masses $0.89+0.46\,M_\odot$ and an initial period of 2.2 days (model 3a), $1.01+0.35\,M_\odot$ and 2.5 days (model 3b), and $0.96+0.35\,M_\odot$ and 2 days (model 3c), each evolved from ZAMS until the present state. We assume a constant mass transfer rate after RLOF of the more massive component around $5.5\text{–}7.7\times 10^{-9}\,M_\odot\,\mathrm{yr}^{-1}$ and a lower rate of $2.9\times 10^{-10}\,M_\odot\,\mathrm{yr}^{-1}$ during the contact phase (see the detailed discussions in Stępień & Kiraga 2015 and in Papageorgiou et al. 2023). At each time step, all stellar parameters are interpolated from the PARSEC (Bressan et al. 2012) grid using the metallicity value of $[\mathrm{Fe/H}]=-1.58\pm 0.10$ dex for CRTS_J163819 from Gaia DR3 (Gaia Collaboration 2022).

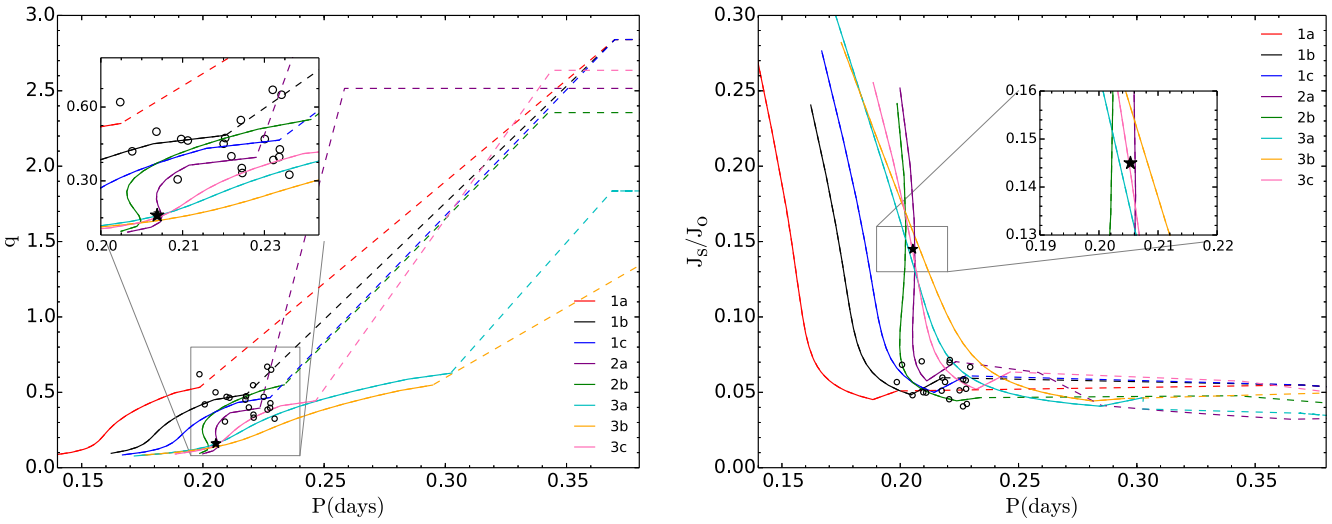

(a) (b)

Figure 4. (a) The mass ratios q and (b) the ratios of spin to orbital AM J_s/J_o of CRTS_J163819 (filled star) and USPCBs (open circles; from Papageorgiou et al. 2023) are plotted as a function of the period P (days), and compared with the various evolutionary models (colored lines, labeled 1a–c, 2a–b, and 3a–c, following the insets) as described in Appendix. Contact phases correspond to the solid lines and precontact phases to the dashed lines.

As seen in Figure 4(a), the progenitors best fitting the present parameters of CRTS_J163819 are described with models 3a and 3b (the cyan and orange lines, respectively). The model progenitors require around 10.7 and 7.2 Gyr, respectively, to match the current properties of the system. As discussed in Papageorgiou et al. (2023), the metallicities of USPCBs tend to be lower than those found in other contact systems, revealing that they are an old population. Due to the absence of additional information (e.g., age), both solutions could be considered equally probable as progenitors. However, there is a weak indication that more extreme mass ratios also come from binaries with more extreme initial mass ratios.

Under this scenario, we consider that the system must first reduce its period near the short limit when it reaches contact, after mass ratio reversal, and later achieve the low mass ratio while it evolves in contact, keeping a constant mass transfer rate. The opposite scenario, in which an LMR contact binary can evolve to a USPCB, does not seem to be plausible, as the mass transfer rate is lower during the contact phase and the latter's mean duration is 0.8–1 Gyr. Even if we consider AM exchange and tidal interaction with a distant tertiary companion, it is difficult for the Kozai–Lidov mechanism (Fabrycky & Tremaine 2007) to reduce dramatically the orbital period of an LMR system. We also display CRTS_J163819 in the $P - J_s/J_o$ plane (Figure 4(b)), together with the above compilation of USPCBs and the above models. It follows from the above approach that further theoretical research is urgently needed to address accurate properties of the ancestors of cool contact EBs, probably through hydrodynamical models and a proper stellar evolution code that includes the contact phase.

ORCID iDs

Athanasios Papageorgiou https://orcid.org/0000-0002-3039-9257
Panagiota-Eleftheria Christopoulou https://orcid.org/0000-0001-6002-7625
C. E. Ferreira Lopes https://orcid.org/0000-0002-8525-7977
Márcio Catelan https://orcid.org/0000-0001-6003-8877
Andrew J. Drake https://orcid.org/0000-0003-0228-6594
Ioannis Alikakos https://orcid.org/0000-0001-6550-1752

References

Applegate, J. H. 1992, ApJ, 385, 621
Bovy, J., Rix, H.-W., Green, G. M., Schlafly, E. F., & Finkbeiner, D. P. 2016, ApJ, 818, 130
Bressan, A., Marigo, P., Girardi, L., et al. 2012, MNRAS, 427, 127
Charbonneau, P. 1995, ApJS, 101, 309
Christopoulou, P.-E., Lalounta, E., Papageorgiou, A., et al. 2022, MNRAS, 512, 1244
Şenavcı, H. V., Doğruel, M. B., Nelson, R. H., Yılmaz, M., & Selam, S. O. 2016, PASA, 33, e043
Drake, A. J., Graham, M. J., Djorgovski, S. G., et al. 2014, ApJS, 213, 9
Eggleton, P. P. 1983, ApJ, 268, 368
Fabrycky, D., & Tremaine, S. 2007, ApJ, 669, 1298
Fonnesbeck, C., Patil, A., Huard, D., & Salvatier, J. 2015, PyMC: Bayesian Stochastic Modelling in Python, Astrophysics Source Code Library, ascl:1506.005
Foreman-Mackey, D., Hogg, D. W., Lang, D., & Goodman, J. 2013, PASP, 125, 306
Foreman-Mackey, D., Price-Whelan, A., Ryan, G., et al. 2014, triangle.py v0.1.1, Zenodo, doi:10.5281/zenodo.11020
Gaia Collaboration 2022, yCat, 1355, 0
Hajdu, T., Borkovits, T., Forgács-Dajka, E., et al. 2019, MNRAS, 485, 2562
Hambálek, Ľ., & Pribulla, T. 2013, CoSka, 43, 27
Heinze, A. N., Tonry, J. L., Denneau, L., et al. 2018, AJ, 156, 241
Hurley, J. R., Tout, C. A., & Pols, O. R. 2002, MNRAS, 329, 897
Hut, P. 1980, A&A, 92, 167
Irwin, J. B. 1952, ApJ, 116, 211
Jayasinghe, T., Kochanek, C. S., Stanek, K. Z., et al. 2018, MNRAS, 477, 3145
Jiang, D. 2020, MNRAS, 492, 2731
Jiang, D., Han, Z., & Li, L. 2014, MNRAS, 438, 859
Lang, D., Hogg, D. W., Mierle, K., Blanton, M., & Roweis, S. 2010, AJ, 139, 1782
Li, K., Kim, C.-H., Xia, Q.-Q., et al. 2020, AJ, 159, 189
Li, K., Xia, Q.-Q., Kim, C.-H., et al. 2021, ApJ, 922, 122
Li, K., Xia, Q.-Q., Michel, R., et al. 2019, MNRAS, 485, 4588
Li, M. C. A., Rattenbury, N. J., Bond, I. A., et al. 2018, MNRAS, 480, 4557
Lucy, L. B. 1967, ZAp, 65, 89
Masci, F. J., Laher, R. R., Rusholme, B., et al. 2019, PASP, 131, 018003
Papageorgiou, A. 2015, PhD thesis, Univ. Patras, doi:10.12681/eadd/35650
Papageorgiou, A., Catelan, M., Christopoulou, P.-E., Drake, A. J., & Djorgovski, S. G. 2021, MNRAS, 503, 2979

Papageorgiou, A., & Christopoulou, P. E. 2015, in ASP Conf. Ser. 496, Living Together: Planets, Host Stars and Binaries, ed. S. M Rucinski, G. Torres, & M. Zejda (San Francisco, CA: ASP), 181
Papageorgiou, A., Christopoulou, P.-E., Ferreira Lopes, C. E., et al. 2023, AJ, 165, 80
Prša, A., Conroy, K. E., Horvat, M., et al. 2016, ApJS, 227, 29
Prša, A., & Zwitter, T. 2005, ApJ, 628, 426
Rasio, F. A. 1995, ApJL, 444, L41
Ruciński, S. M. 1973, AcA, 23, 79
Rucinski, S. M. 1992, AJ, 103, 960
Rucinski, S. M. 2020, AJ, 160, 104
Science Software Branch at STScI 2012, PyRAF: Python alternative for IRAF, Astrophysics Source Code Library, ascl:1207.011
Shappee, B. J., Prieto, J. L., Grupe, D., et al. 2014, ApJ, 788, 48
Stassun, K. G., Oelkers, R. J., Paegert, M., et al. 2019, AJ, 158, 138
Stępień, K., & Kiraga, M. 2015, A&A, 577, A117
Stepien, K. 1995, MNRAS, 274, 1019
Stepien, K. 2006, AcA, 56, 347
Terrell, D., & Wilson, R. E. 2005, Ap&SS, 296, 221
Tian, Y. P., Xiang, F. Y., & Tao, X. 2009, Ap&SS, 319, 119
Tylenda, R., Hajduk, M., Kamiński, T., et al. 2011, A&A, 528, A114
van Hamme, W. 1993, AJ, 106, 2096
Völschow, M., Schleicher, D. R. G., Perdelwitz, V., & Banerjee, R. 2016, A&A, 587, A34
Wadhwa, S. S., De Horta, A., Filipović, M. D., et al. 2021, MNRAS, 501, 229
Wilson, R. E., & Biermann, P. 1976, A&A, 48, 349
Wilson, R. E., & Devinney, E. J. 1971, ApJ, 166, 605
Wilson, R. E., Devinney, E. J., & Van Hamme, W. 2020, WD: Wilson-Devinney binary star modeling, Astrophysics Source Code Library, ascl:2004.004
Yakut, K., & Eggleton, P. P. 2005, ApJ, 629, 1055
Zasche, P., Wolf, M., Vraštil, J., et al. 2014, A&A, 572, A71